RANDGAN: RANDOMIZED GENERATIVE ADVERSARIAL NETWORK FOR DETECTION OF COVID-19 IN CHEST X-RAY

A PREPRINT

Saman Motamed
sam.motamed@mail.utoronto.ca

Patrik Rogalla
patrik.rogalla@uhn.ca

Farzad Khalvati
farzad.khalvati@utoronto.ca

Intelligent Medical Image Computing Systems (IMICS) Lab
www.imics.ca
Department of Medical Imaging
The Hospital for Sick Children
University of Toronto
Toronto, Ontario, Canada

October 14, 2020

ABSTRACT

COVID-19 spread across the globe at an immense rate has left healthcare systems incapacitated to diagnose and test patients at the needed rate. Studies have shown promising results for detection of COVID-19 from viral bacterial pneumonia in chest X-rays. Automation of COVID-19 testing using medical images can speed up the testing process of patients where health care systems lack sufficient numbers of the reverse-transcription polymerase chain reaction (RT-PCR) tests. Supervised deep learning models such as convolutional neural networks (CNN) need enough labeled data for all classes to correctly learn the task of detection. Gathering labeled data is a cumbersome task and requires time and resources which could further strain health care systems and radiologists at the early stages of a pandemic such as COVID-19. In this study, we propose a randomized generative adversarial network (RANDGAN) that detects images of an unknown class (COVID-19) from known and labelled classes (Normal and Viral Pneumonia) without the need for labels and training data from the unknown class of images (COVID-19). We used the largest publicly available COVID-19 chest X-ray dataset, COVIDx, which is comprised of Normal, Pneumonia, and COVID-19 images from multiple public databases. In this work, we use transfer learning to segment the lungs in the COVIDx dataset. Next, we show why segmentation of the region of interest (lungs) is vital to correctly learn the task of classification, specifically in datasets that contain images from different resources as it is the case for the COVIDx dataset. Finally, we show improved results in detection of COVID-19 cases using our generative model (RANDGAN) compared to conventional generative adversarial networks (GANs) for anomaly detection in medical images, improving the area under the ROC curve from 0.71 to 0.77.

Keywords Generative Adversarial Networks · COVID-19 Detection · Semi-supervised Anomaly Detection

1 Introduction

COVID-19 spread globally over a short period of time and became a deadly pandemic [1]. Early diagnosis and detection of pneumonia can minimize the risk factors of the illness [2] and help break the transmission chain. The standard test for diagnosis of COVID-19 is reverse transcriptase polymerase chain reaction (RT-PCR) [3]. The lack of accessibility

and slowness of RT-PCR, along with its high false negative rate $39 - 61\%$, drew attention to diagnosis of COVID-19 using chest radiographs [4, 5]. Automation of COVID-19 diagnosis using chest X-rays can help healthcare systems keep up with demands for patients testing as X-rays are more readily available than RT-PCR and reduce strain from radiologists and healthcare systems. Medical imaging based diagnosis can also help control the high false negative rate of RT-PCR tests by acting as a secondary control. Computer-aided disease diagnosis using medical imaging techniques have accelerated over the past decade due to the breakthroughs in the field of Machine Learning and the development of detection and classification models that are based on Convolutional Neural Networks (CNNs) [6–8]. CNNs, which are mainly used in supervised frameworks, require large amounts of labeled data to learn the task of anomaly detection, such as detecting COVID-19 in chest X-rays. Supervised architectures require training data with complete labels for all image classes (e.g., normal and COVID-19). Nevertheless, this requires accurate labeling of the data for all cases and the cumbersome annotation effort, and the diagnosis variation amongst expert radiologists limits the performance of these supervised models on new data. Specially, in pandemics such as COVID-19, at the beginning, there is limited COVID-19 data (if any data at all) available for training a supervised classification model. In contrast, solutions based on semi-supervised learning only require partial labels for the training data [9]. Semi-supervised learning significantly reduces the cost of creating training data and ,thus, opens new opportunities for automated disease detection using training data with only single class labels.

In this study, we propose a semi-unsupervised generative model (RANDGAN) for detection of COVID-19 positive chest X-ray images. The idea behind anomaly detection using generative adversarial networks (GANs) comes from the great ability of generative models in learning the image-space manifold where training images lie on, and being able to generate never-before-seen images that lie on the learned image-space [10]. Anomaly detection may be seen as only detecting abnormality in medical images such as a tumour or pneumonia. We extend the definition of anomaly in medical images as the deviation from the image-space manifold of training data. In other words, if the training data only includes COVID-19 negative cases (i.e., healthy or viral pneumonia), the anomaly detected in test cases is indeed an abnormality such as COVID-19. On the other hand, if the training data only includes COVID-19 positive cases, the "anomaly" detected in the test cases are the deviation from COVID-19 cases, meaning that the test case does not contain the abnormality in the training class (i.e., healthy or viral pneumonia). We show our proposed RANDGAN model is able to differentiate between COVID-19 positive and negative images. To the best of our knowledge, this study is the first of its kind, using semi-supervised learning for detection of COVID-19 in medical images and reporting performance accuracy on the entire cohort of COVID-19 positive images without the need to use any of the COVID-19 positive images to train our model.

2   Dataset

Covid-chestxray dataset [11] is an effort by Cohen *et al.* to make a public COVID-19 dataset of chest X-ray images with normal, pneumonia, and COVID-19 radiological readings. Wang *et al.* uses covid-chestxray dataset, along with four other publicly available datasets and compiles COVIDx [12] dataset. With the number of images growing, many deep learning models are trained and tested on this public dataset [12–14]. Figure 1 shows the class distribution of the COVIDx dataset. The images are in RGB format, with pixel range of $[0, 255]$ and have various sizes. To train the generative models in this study, all images were converted to gray scale, resized to 128×128 pixels and normalized to have pixel intensities in the $[-1, 1]$ range.
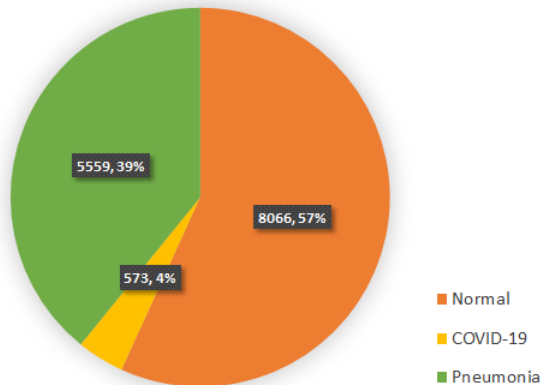

Figure 1: Class distribution of COVIDx dataset

3   Related Work

Using the covid-chestxray and COVIDx datasets, multiple studies have utilized supervised deep learning models to detect COVID-19 in chest X-rays [12–17]. Wang *et al.*'s CNN based COVID-NET [12] achieved a 93.3% test accuracy for multi-class classification on a test cohort of 100 Normal, 100 Pneumonia and 100 COVID-19 from the COVIDx dataset with the rest of images of each class being used to train their model. Hemdan *et al.*'s COVIDX-Net [16], comprised of multiple architectures such as VGG19, DenseNet121 and InceptionV3, was tested on a small set of 50 X-ray images from the covid-chestxray dataset. 25 COVID-19 positive and 25 COVID-19 negative. They report accuracy of anywhere between 50% (InceptionV3) to 90% (VGG19 and DenseNet201) for each investigated architecture. Ozturk *et al.*'s DarkNet [13] experimented with both binary classification (COVID-19 vs. No Findings) and multi-class classification (Pneumonia vs. COVID-19 vs. No Findings). They report a binary classification accuracy of 98.08 % and multi-class classification with accuracy of 0.87% on 25 COVID-19, 100 Normal and 100 Pneumonia images. Afshar *et al.* proposed using capsule networks for binary classification of COVID-19 positive and negative cases using COVIDx dataset, pre-trained on non-COVID chest X-ray images from other datasets. They report an Accuracy of 95.7%, Sensitivity of 90%, Specificity of 95.8%, and the area under the ROC curve (AUC) of 0.97. The number of test images from each class is not disclosed in their paper.

The high accuracy achieved in these models, despite the imbalanced dataset with only 4% of the images belonging to COVID-19 and the multi-centric nature of the dataset which could cause images from different scanners and health centres to have inherent difference in characteristics, put the robustness of these models under question. Another issue is transparency in number of test images used in these studies where the train and test split of the dataset used in the experiments is not clear.

DeGrave *et al.* [18] conducted a few experiments to test the generalizability and robustness of these models trained on the COVIDx dataset. Replicating different supervised models such as COVID-NET [12] and training the models on COVIDx dataset, they achieve high test accuracy when tested on COVIDx data. Their predictive performance, however, drops by 50% when they validate their model on an external COVID and Non-COVID dataset [19] where the images are from a single institute. Furthermore, using saliency maps, which highlight the region of each X-ray image that contributed most to the classification decision of the CNNs, they find non-COVID markers such as image edges, diaphragm and cardiac silhouette have contributed to the classification of COVID-19; markers that do not have a predictive value for detection of COVID-19 [20]. This confirms that using the full images from a dataset that comes from different scanners can be problematic where non-disease specific markers could act as a shortcut [21] and help CNNs achieve high accuracy on a particular dataset yet fail to generalize to any other dataset. To minimize the effect of shortcuts, we create a segmented COVIDx dataset that includes only the lungs where the true markers of COVID-19 and Pneumonia appear.

4   Segmentation of Lung in COVIDx Images

To mitigate the issue of deep learning models picking non-disease related markers from the images, we created a new dataset by segmenting the lungs of COVIDx dataset. As the training set, we used the Montgomery County chest X-ray set [22], which contains 138 frontal chest X-rays from Montgomery County's Tuberculosis screening program with corresponding masks manually annotated radiologists. We resized the images to 256×256 pixels and normalized to have pixel intensities between 0 and 1. We trained a U-NET [23] based model, that has been augmented with Inception and Residual architectures, with these normalized images [24, 25]. Transfer learning [26] has shown promise in adapting tasks from one domain (source) to another (target). For the task of lung segmentation for COVIDx dataset, the Montgomery dataset was used as the source and COVIDx as the target domains. For the task of transfer learning, Sefexa [27], an image segmentation tool, was used for manual segmentation of 900 randomly selected images of the COVIDx dataset. All segmentation masks were corrected by an experienced radiologist and intentionally over-segmented to ensure no region of lung is excluded. Thus, these masks are best to be used for classification algorithms for detection of COVID-19 and pneumonia, and not for precise segmentation of lung boundaries. 850 segmented X-ray images from COVIDx were used for performing transfer learning [24] from the Montgomery dataset to COVIDx. We kept 50 manual segmentations to evaluate our model's accuracy. Since source domain is smaller than our target domain, we fine-tuned 75% of the pre-trained model's layers (encoder part), and trained on the Montgomery dataset images. We froze the first 25% layers of the pre-trained U-NET and fine-tuned the rest of the encoder and decoder components based on our manual segmentation for COVIDX images. We used open and close operations as a post-processing step to fill any holes in the masks and reduce noise in the predicted masks. We tested the accuracy of our model using Sørensen–Dice coefficient (DSC). We achieved a DSC of 0.83 on our test set of 50 images.

Figure 2 shows the output of our segmentation model. We include some of the failed segmentation attempts of the model as well. Accurate segmentation of lung images are a limitation of using automated segmentation models.
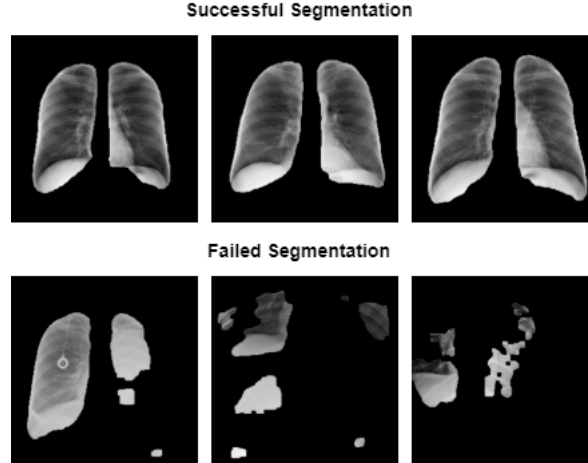
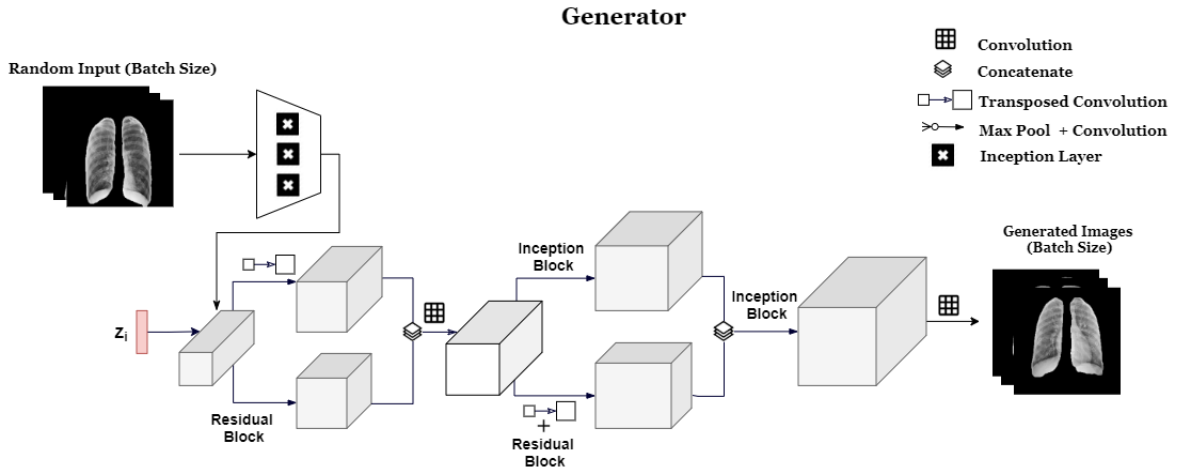Figure 2: Output samples of our segmentation model on COVIDx images

Figure 3: RANDGAN's Generator Architecture

5 Random Input Generative Adversarial Networks

Generative Adversarial Networks (GANs) [10] revolutionized the field of deep learning by allowing generation of never-before-seen data that follows the distribution of real data. Applications of GANs have expanded from generating human-like faces, to image style transfer and detection of anomalies in images [28]. Below we describe the components of our proposed Random Input Generative Adversarial Networks (RANDGAN).

5.1 Generator Network

The Generator ($\mathbf{G}$) (Fig. 3) learns a distribution P_g over the input data x via mapping of input noise z, to $2D$ images by function $G(z)$. The trained Generator learns the mapping $G(z) : z \longmapsto x$ from latent space representations z to realistic, $2D$, X-ray images. Our Generator model follows DCGAN's architecture (named AnoGAN for anomaly detection GAN in the study) [28] (used for anomaly detection for retina) with three main modifications; the use of randomized 2D image inputs to the generator, inception layers, and residual connections as shown in Fig. 4.

Feeding real training image as an input to the generator has shown improvement in using GANs for augmenting images [29, 30]. Real image is encoded into a lower dimensional space before being concatenated with the noise input vector z. To improve generalizability of our generator, specially due to the multi-centric nature of COVIDx data, we randomly select $batch - size$ images from the cohort of our training class and encode them to a lower-representation space using inception layers. This helps in adding variability to each iteration of the generator's training by not only using a random noise vector, but also real, random image representations of the training class. Doing so shows improved
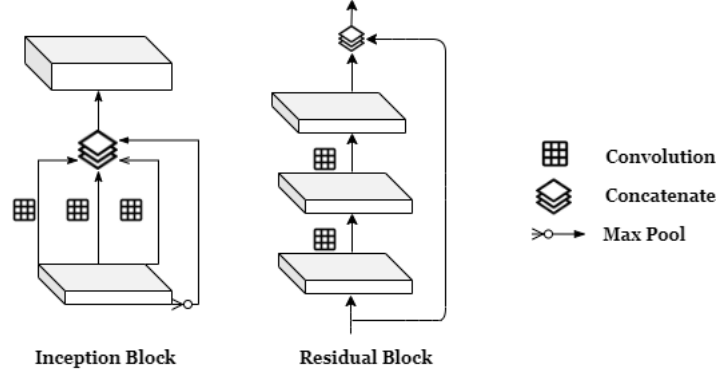
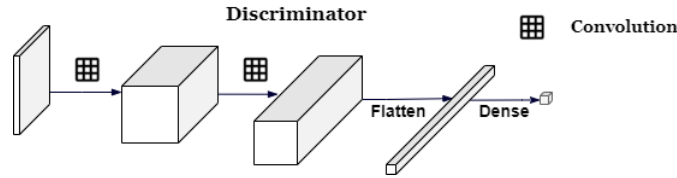Figure 4: Inception and Residual Block Architecture

Figure 5: RANDGAN's Discriminator Architecture

results when using the trained GAN to classify images of class c from other classes. The idea behind the inception and residual architecture [31] is being able to increase GAN's ability to capture more details from training image-space without losing spatial information after each convolution and pooling layer. Although making the Generator deeper is theoretically a valid way to capture more long-range details in the image, deep GANs are unstable and hard to train [28, 32].

5.2 Discriminator

The Discriminator (**D**) (Fig. 5) is a 4-layer CNN that maps a 2D image to a scalar output that can be interpreted as the probability of the given input being a real chest X-ray sampled from training data or generated G(z) by the Generator G.

Optimization of D and G can be thought of as the following game of minimax [10] with the value function $V(G, D)$:

$$\min_G \max_D V(D, G) = \mathbb{E}_{x \sim P_{data(x)}} \left[\log D(x) \right] + \mathbb{E}_{z \sim P_{z(z)}} \left[\log(1 - D(G(z))) \right] \tag{1}$$

During training, Generator G is trained to minimize the accuracy of Discriminator D's ability in distinguishing between real and generated images while the Discriminator is trying to maximize the probability of assigning real training images the "real" and generated images from G, "fake" labels. The Generator improves at generating more realistic images while Discriminator gets better at correctly identifying between real and generated images.

6 Experiments

6.1 Data and Pre-processing

We used both full images from COVIDx dataset and our segmentation of the COVIDx data to train separate models and compare the results. One of the advantages of our semi-supervised model compared to supervised models is the ability to test our model on not only a subset, but all of COVID-19 positive images as we do not use any of the images to train our model. While studies such as Wang et. al's COVID-NET use 100 images of COVID-19, Hedman *et al.* [16] and Ozturk *et al.* [13] using 25 COVID-19 positive images to test their models, we used 573 images of each class; the entire dataset for COVID-19 was used and for normal and pneumonia classes, 573 images were randomly selected for each class. All images, converted from RGB to grayscale, were resized to 128×128 pixels, with pixel intensities normalized to have values between -1 and 1. tHe models were trained using an NVIDIA GeForce RTX 2080 Ti with 11 GB of memory.

Table 1 shows the Train and Test split of our COVIDx and Segmented COVIDx images.

Table 1: Train and Test class distribution of COVIDx and COVIDx segmentation dataset

Label	Train	Test
Normal	7,493	573
Pneumonia	4,986	573
COVID-19	N/A	573

6.2   Evaluation

We trained two instances of our RANDGAN. For comparison, we repeated the same training using the GAN model (AnoGAN) used in Radford et. al's [28] anomaly detection study. One RANDGAN / AnoGAN was trained using Normal images and the other RANDGAN / AnoGAN was trained using Pneumonia images. When the model's training is done, the Generator has learned the mapping $G(z) : z \longmapsto x$ from latent space representation z to realistic images (Chest X-ray with Pneumonia). Given a query image x in test, we want to find a point z from the latent space that, given the Generator's output on that point ($G(z)$), that is most similar to the query image x. The expected behaviour after successful training is that the query image x, if affected by pneumonia, will result in finding an image $G(z)$, which is visually closer to image x than if the query image was a normal case.

To find latent variable z that generates the most similar image $G(z)$ to the query image x, we used back propagation with a predefined number of steps. The loss function defined to find such z through back-propagation is comprised of two components; *residual loss* and *discrimination loss*. Residual loss ($\mathcal{L}_\mathcal{R}$) calculates the L1 distance between $G(z)$ and the query image x and enforces visual similarity between the query image and generated image.

$$\mathcal{L}_R(z_i) = \sum |x - G(z_i)| \tag{2}$$

Schlegl *et al.* [33] proposed a discrimination loss ($\mathcal{L}_\mathcal{D}$) inspired by the concept of feature matching [?] that enforces generated images $G(z_i)$ to follow the statistical characteristics of the training images. $\mathcal{L}_\mathcal{R}$ is defined below where the output of an intermediate layer of the discriminator, $f(.)$, is used to represent the statistical characteristics of the input image.

$$\mathcal{L}_D(z_i) = \sum |f(x) - f(G(z_i))| \tag{3}$$

The overall loss used to back-propagate and find the best z is a weighted sum of residual and discrimination loss;

$$\mathcal{L}(z_i) = (1 - \lambda) \times \mathcal{L}_R(z_i) + \lambda \times \mathcal{L}_D(z_i) \tag{4}$$

The Anomaly score $A(x)$ for the query image x is defined as;

$$A(x) = (1 - \lambda) \times R(x) + \lambda \times D(x) \tag{5}$$

where R(x) and D(x) are respectively the residual and discrimination loss of the best z_i found through back-propagation. λ adjusts the weighted sum of the overall loss and anomaly score. We used $\lambda = 0.2$ to train our proposed RANDGAN and AnoGAN [33]. Both architectures were trained with the same initial conditions for performance comparison.

With two trained models, one on Normal and one on Pneumonia images, we calculate two anomaly scores 5 for each test image. One anomaly score from inputting the test image into Normal trained GAN and one from Pneumonia trained GAN. The anomaly score generated from the Normal trained GAN will be lower for Normal test images compared to Pneumonia and COVID-19 images. Respectively, the anomaly score generated from Pneumonia trained GAN will be lower for Pneumonia test images compared to Normal and COVID-19 images. For each test image and the corresponding two anomaly scores, we generate a single anomaly score by summing the two scores together. The idea is that COVID-19 (unknown) images would score high anomalies from both networks while Normal and Pneumonia images score low in one model and high in the other. This should lead to the COVID-19 (unknown) images to score higher overall than the two other (known) classes.

7   Results

We generated a single anomaly score, comprised of two anomaly scores from the two trained models (Normal, Pneumonia), for the images in our test set. 573 anomaly scores were computed for each class (Normal, Pneumonia and COVID-19) of our COVIDx and segmented COVIDx dataset. To evaluate the performance of our COVID-19 positive detection model on a balanced test set, we randomly selected 286 Normal labeled and 287 Pneumonia labeled images

and combine them into a COVID-19 negative test set with corresponding anomaly scores. We repeated the random selection of images from Normal and Pneumonia test cohorts 5 times in order to achieve an average performance metric of our models. The experiments were performed using AnoGAN trained on full COVIDx images, AnoGAN trained on segmented COVIDx images and RANDGAN on segmented COVIDx images. Table 2 shows the average AUC of our models for the 5 calculations. We also report the AUC on the unbalanced test set, using 573 COVID-19 positive and 1146 COVID-19 negative (573 normal and 573 Pneumonia) images.

Table 2: Performance comparison of RANDGAN and AnoGAN

Model	Dataset	AUC
AnoGAN	COVIDx (Balanced test set)	0.54
AnoGAN	Segmented COVIDx (Balanced test set)	0.71
RANDGAN	Segmented COVIDx (Balanced test set)	**0.77**
RANDGAN	Segmented COVIDx (Imbalanced test set)	0.76

Figure 6 shows the Receiver operating characteristic (**ROC**) curve of the 3 trained models.
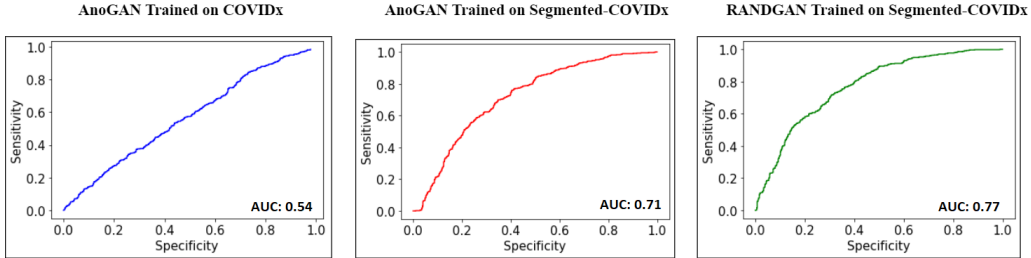

Figure 6: ROC curve of the trained generative models

Figure 7 shows the normalized average anomaly score of the 5 runs of each of our three models; RANDGAN trained on segmented X-ray images, AnoGAN trained on segmented images and AnoGAN trained on full images. Despite the ROC curve that combines a balanced number of Normal and Pneumonia images in comparison to COVID-19 images, we present the anomaly scores in their entirety (573 Normal, 573 Pneumonia and 573 COVID-19 images). RANDGAN shows the biggest gap of normalized mean anomaly score (MAS) between COVID-19 (MAS = 4.48) and Pneumonia (3.01) and COVID-19 and Normal (3.56) images which are 1.47 and 0.92 respectively. AnoGAN trained on segmented COVIDx dataset shows 1.36 as the gap between COVID-19 (MAS = 4.42) and 0.91 between COVID-19 and Normal (3.51). AnoGAN trained on full COVIDx images shows a small gap between COVID-19, Pneumonia and Normal images (0.36 between COVID-19 and Pneumonia and 0.12 between COVID-19 and Normal).

8   Discussion

In this study, we introduced RANDGAN, a novel generative adversarial network for semi-supervised detection of an unknown (COVID-19) class in chest X-ray images from a pool of known (Normal and Pneumonia) and unknown classes (COVID-19) by only using the known classes for training. With this model, unknown cases can be screened and flagged for further investigations by radiologists increasing the probability of catching such cases early on. Using semi-supervised approaches for a problem such as detection of COVID-19, specially at the beginning of a pandemic are preferred over supervised approaches for they allow faster training of models without the need for gathering and annotation of data from the spreading disease. The result of semi-supervised models are also more robust where number of images are limited for the unknown (COVID-19) class because all images can be used to test the model where supervised models have to use majority of the images for training the model and test the model on a small subset of the images.

We also showed the importance of segmentation of lungs for the COVIDx dataset. DeGrave *et al.* [18] showed non-disease markers outside the lung act as shortcuts [21] in helping CNNs performance on specific datasets on which, the model is trained. By using transfer learning and segmenting the lung, we showed that using lung only images boosts the performance of generative models in detecting COVID-19 from Pneumonia and Normal images. AnoGAN [28] achieved an average AUC of 0.54 when using full images from COVIDx images while using segmented COVIDx images achieved an average AUC of 0.71.
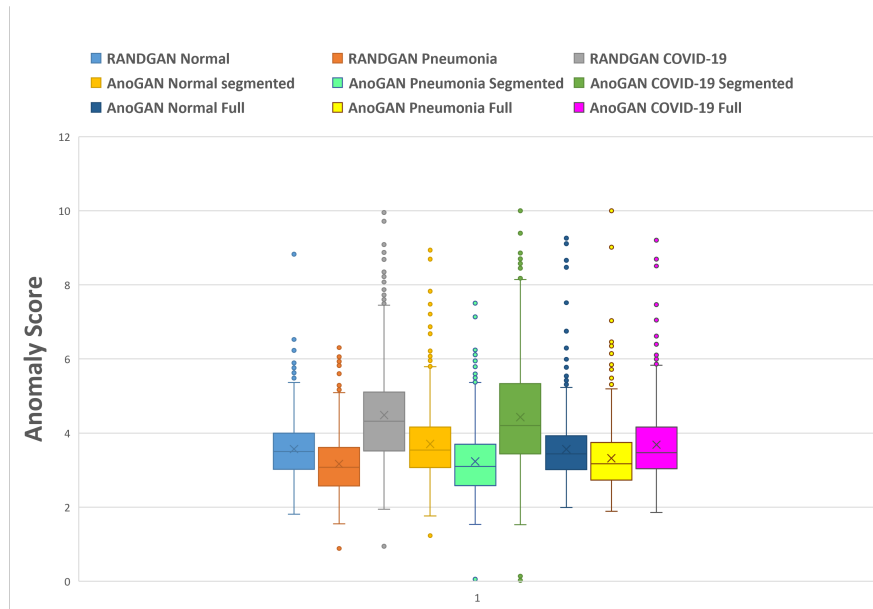
Figure 7: Normalized average anomaly score of the trained generative models

Future directions will focus on improving the performance of our proposed RANDGAN (AUC of 0.77) model by performing data augmentation and as more data is collected, it is important to validate the model on external data sources.

9 Limitations

One limitation of working with data of relatively early stages of a disease such as COVID-19 is dataset size. Even though our semi-supervised model is able to use all COVID-19 images to evaluate the performance of the model, while supervised models have to use majority of the already small COVID-19 cohort to train their images, more images would allow for a better understanding of the true performance of both supervised and semi-supervised models. Segmentation accuracy of the lungs is another limiting factor. Although the performance of the base model greatly improves (AUC of 0.54 to 0.71), segmentation model fails in some cases (Figure 2). As more data gets collected and becomes available from different health care systems, any model trained for detection of COVID-19 needs validation from external sources. Without validation, these models need to be used as a secondary measure for detection of COVID-19.

References

[1] Rong-Hui Du, Li-Rong Liang, Cheng-Qing Yang, Wen Wang, Tan-Ze Cao, Ming Li, Guang-Yun Guo, Juan Du, Chun-Lan Zheng, Qi Zhu, et al. Predictors of mortality for patients with covid-19 pneumonia caused by sars-cov-2: a prospective cohort study. *European Respiratory Journal*, 55(5), 2020.

[2] Jose Manuel Pereira, Jose Artur Paiva, and Jordi Rello. Severe sepsis in community-acquired pneumonia—early recognition and treatment. *European journal of internal medicine*, 23(5):412–419, 2012.

[3] Wenling Wang, Yanli Xu, Ruqin Gao, Roujian Lu, Kai Han, Guizhen Wu, and Wenjie Tan. Detection of sars-cov-2 in different types of clinical specimens. *Jama*, 323(18):1843–1844, 2020.

[4] Shinjini Kundu, Hesham Elhalawani, Judy W Gichoya, and Charles E Kahn Jr. How might ai and chest imaging help unravel covid-19's mysteries?, 2020.

[5] Lauren Kucirka, Stephen Lauer, Oliver Laeyendecker, Denali Boon, and Justin Lessler. Variation in false negative rate of rt-pcr based sars-cov-2 tests by time since exposure. *medRxiv*, 2020.

[6] Jonathan Long, Evan Shelhamer, and Trevor Darrell. Fully convolutional networks for semantic segmentation. In *The IEEE Conference on Computer Vision and Pattern Recognition (CVPR)*, June 2015.

[7] Ross Girshick. Fast r-cnn. In *Proceedings of the IEEE international conference on computer vision*, pages 1440–1448, 2015.

[8] Alex Krizhevsky, Ilya Sutskever, and Geoffrey E Hinton. Imagenet classification with deep convolutional neural networks. In *Advances in neural information processing systems*, pages 1097–1105, 2012.

[9] Xiaojin Zhu and Andrew B Goldberg. Introduction to semi-supervised learning. *Synthesis lectures on artificial intelligence and machine learning*, 3(1):1–130, 2009.

[10] Ian Goodfellow, Jean Pouget-Abadie, Mehdi Mirza, Bing Xu, David Warde-Farley, Sherjil Ozair, Aaron Courville, and Yoshua Bengio. Generative adversarial nets. In *Advances in neural information processing systems*, pages 2672–2680, 2014.

[11] Joseph Paul Cohen, Paul Morrison, and Lan Dao. Covid-19 image data collection. arxiv 2003.11597, 2020. *URL https://github. com/ieee8023/covid-chestxray-dataset*, 2020.

[12] Linda Wang and Alexander Wong. Covid-net: A tailored deep convolutional neural network design for detection of covid-19 cases from chest x-ray images. *arXiv preprint arXiv:2003.09871*, 2020.

[13] Tulin Ozturk, Muhammed Talo, Eylul Azra Yildirim, Ulas Baran Baloglu, Ozal Yildirim, and U Rajendra Acharya. Automated detection of covid-19 cases using deep neural networks with x-ray images. *Computers in Biology and Medicine*, page 103792, 2020.

[14] Parnian Afshar, Shahin Heidarian, Farnoosh Naderkhani, Anastasia Oikonomou, Konstantinos N Plataniotis, and Arash Mohammadi. Covid-caps: A capsule network-based framework for identification of covid-19 cases from x-ray images. *arXiv preprint arXiv:2004.02696*, 2020.

[15] Md Karim, Till Döhmen, Dietrich Rebholz-Schuhmann, Stefan Decker, Michael Cochez, Oya Beyan, et al. Deep-covidexplainer: Explainable covid-19 predictions based on chest x-ray images. *arXiv preprint arXiv:2004.04582*, 2020.

[16] Ezz El-Din Hemdan, Marwa A Shouman, and Mohamed Esmail Karar. Covidx-net: A framework of deep learning classifiers to diagnose covid-19 in x-ray images. *arXiv preprint arXiv:2003.11055*, 2020.

[17] Biraja Ghoshal and Allan Tucker. Estimating uncertainty and interpretability in deep learning for coronavirus (covid-19) detection. *arXiv preprint arXiv:2003.10769*, 2020.

[18] Alex J DeGrave, Joseph D Janizek, and Su-In Lee. Ai for radiographic covid-19 detection selects shortcuts over signal. *medRxiv*, 2020.

[19] Maria de la Iglesia Vayá, Jose Manuel Saborit, Joaquim Angel Montell, Antonio Pertusa, Aurelia Bustos, Miguel Cazorla, Joaquin Galant, Xavier Barber, Domingo Orozco-Beltrán, Francisco Garcia, et al. Bimcv covid-19+: a large annotated dataset of rx and ct images from covid-19 patients. *arXiv preprint arXiv:2006.01174*, 2020.

[20] Ming-Yen Ng, Elaine YP Lee, Jin Yang, Fangfang Yang, Xia Li, Hongxia Wang, Macy Mei-sze Lui, Christine Shing-Yen Lo, Barry Leung, Pek-Lan Khong, et al. Imaging profile of the covid-19 infection: radiologic findings and literature review. *Radiology: Cardiothoracic Imaging*, 2(1):e200034, 2020.

[21] Robert Geirhos, Jörn-Henrik Jacobsen, Claudio Michaelis, Richard Zemel, Wieland Brendel, Matthias Bethge, and Felix A Wichmann. Shortcut learning in deep neural networks. *arXiv preprint arXiv:2004.07780*, 2020.

[22] Stefan Jaeger, Sema Candemir, Sameer Antani, Yì-Xiáng J Wáng, Pu-Xuan Lu, and George Thoma. Two public chest x-ray datasets for computer-aided screening of pulmonary diseases. *Quantitative imaging in medicine and surgery*, 4(6):475, 2014.

[23] Olaf Ronneberger, Philipp Fischer, and Thomas Brox. U-net: Convolutional networks for biomedical image segmentation. *Medical Image Computing and Computer-Assisted Intervention – MICCAI 2015*, page 234–241, 2015.

[24] Saman Motamed, Isha Gujrathi, Dominik Deniffel, Anton Oentoro, Masoom A Haider, and Farzad Khalvati. A transfer learning approach for automated segmentation of prostate whole gland and transition zone in diffusion weighted mri. *arXiv preprint arXiv:1909.09541*, 2019.

[25] Tyler Clark, Alexander Wong, Masoom A Haider, and Farzad Khalvati. Fully deep convolutional neural networks for segmentation of the prostate gland in diffusion-weighted mr images. In *International Conference Image Analysis and Recognition*, pages 97–104. Springer, 2017.

[26] Chuanqi Tan, Fuchun Sun, Tao Kong, Wenchang Zhang, Chao Yang, and Chunfang Liu. A survey on deep transfer learning. In *International conference on artificial neural networks*, pages 270–279. Springer, 2018.

[27] Ales Fexa. *Sefexa Image Segmentation Tool*.

[28] Alec Radford, Luke Metz, and Soumith Chintala. Unsupervised representation learning with deep convolutional generative adversarial networks. *arXiv preprint arXiv:1511.06434*, 2015.

[29] Antreas Antoniou, Amos Storkey, and Harrison Edwards. Data augmentation generative adversarial networks. *arXiv preprint arXiv:1711.04340*, 2017.

[30] Saman Motamed and Farzad Khalvati. Inception augmentation generative adversarial network, 2020.

[31] Christian Szegedy, Vincent Vanhoucke, Sergey Ioffe, Jon Shlens, and Zbigniew Wojna. Rethinking the inception architecture for computer vision. In *Proceedings of the IEEE conference on computer vision and pattern recognition*, pages 2818–2826, 2016.

[32] Naveen Kodali, Jacob Abernethy, James Hays, and Zsolt Kira. On convergence and stability of gans. *arXiv preprint arXiv:1705.07215*, 2017.

[33] Thomas Schlegl, Philipp Seeböck, Sebastian M Waldstein, Ursula Schmidt-Erfurth, and Georg Langs. Unsupervised anomaly detection with generative adversarial networks to guide marker discovery. In *International conference on information processing in medical imaging*, pages 146–157. Springer, 2017.